

# Observations of Tropical Cirrus Properties in the Pilot Radiation Observation Experiment Using Lidar and the CSIRO ARM Filter Radiometer

C.M.R. Platt, S. A. Young, P. J. Manson, and G. R. Patterson  
CSIRO Division of Atmospheric Research  
Station Street, Aspendale, Victoria, Australia

A narrow beam fast filter radiometer has been developed for the Atmospheric Radiation Measurement (ARM) Program. The radiometer is intended to operate alongside a lidar at ARM sites in a lidar/radiometer (LIRAD) configuration. The radiometer detects in three narrow bands at 8.62-, 10.86-, and 12.04- $\mu$ m central wavelengths in the atmospheric window. In addition, it has a variable field aperture that varies the radiance incident on the detector and also allows the field of view to be tailored to that of a lidar used in the LIRAD technique.

The radiometer was deployed in the ARM Pilot Radiation Observation Experiment (PROBE) at Kavieng, Papua New Guinea in January-February 1993. The radiometer worked satisfactorily and appeared to be very stable. The radiometer was compared with a previous CSIRO radiometer and the improved performance of the ARM instrument was very evident. The ARM radiometer was also compared with a National Oceanic and Atmospheric Administration (NOAA) Environmental Technology Laboratories (ETL) interferometer and gave closely equivalent radiances.

The LIRAD method was used at Kavieng to obtain the optical properties of cirrus clouds. Continuous observations of water vapor path obtained by the NOAA ETL microwave radiometer were employed to allow for the strong tropical water vapor absorption and emission.

Cirrus cells that developed on one morning, independent of other clouds, had measured infrared emittances varying from  $<0.1$  to  $1.0$ .

## Introduction

The aim of the ARM filter radiometer development program was to produce a sensitive radiometric instrument to use in parallel with a lidar in the LIRAD technique of obtaining

the optical properties of high clouds in a column of atmosphere over the measurement site (e.g., Platt et al. 1987). The LIRAD method retrieves the optical depths of cirrus clouds at the radiometer infrared and lidar visible wavelengths. The optical depths at other wavelengths in the infrared and visible regions can then be calculated from theoretical considerations, after which the total effect of the specific cloud can be calculated (e.g., Platt and Harshvardhan 1988).

The radiative divergence in a column of atmosphere can similarly be obtained in near real-time. Statistics of the above quantities can be gathered over suitably long periods of time to yield a data set both for improving numerical model parameterizations and for validating subsequent predictions.

## The ARM Filter Radiometer

The design and construction of the ARM radiometer have been described in Platt et al. (1994). Here, we give a brief description. The radiometer optical system is Newtonian with a spherical primary mirror and plane secondary mirror. A beam selector consisting of a reflecting  $45^\circ$  mirror at the input selects either a blackbody at liquid nitrogen temperature, an ambient temperature blackbody, or a view of the sky at a selected angle between the horizontal and vertical directions.

The beam then passes through an aperture consisting of two opposite quadrants. The opposing two quadrants contain a grooved blackbody on the side facing the primary mirror and are heated by a novel heater coil attached to the back. The heater consists of an ultra-thin printed circuit board, the circuit consisting of copper looped many times to form a resistor of 10 ohms and etched on to a Mylar plastic film.

The grooved aperture blackbody is chopped at 100 Hz by a two-bladed chopper on the side facing the primary mirror to ensure that radiation from the chopper blades does not vary over one cycle. When the blades cover the aperture quadrants, the primary mirror views radiation from the blackbody. In the other position, the mirror views sky radiation. After the primary mirror, the radiation is reflected through 90 degrees by a plane mirror and focused onto the field aperture. This aperture consists of a variable iris which gives an effective aperture of between 3 and 30 milliradians. The radiation is then collimated and reflected through 90 degrees by an off-axis paraboloid, passed through a narrow-band optical filter, and focused onto a liquid-nitrogen-cooled mercury cadmium telluride (HgCdTe) photo detector. The detected alternating signal is amplified by a low-noise amplifier, which is integral with the detector. The signal is then further amplified and synchronously rectified using an in-phase signal of the same frequency derived from a chopper photodiode.

The filter wheel allows the choice of three spectral pass bands at 8.62, 10.86 and 12.04  $\mu\text{m}$ , respectively, and half widths of about 0.5  $\mu\text{m}$ . A fourth filter window allows a view of the spectral region from 8 to 13  $\mu\text{m}$  whose width is determined by a bandpass filter that is integral with the HgCdTe detector. The filter wheel, aperture iris, and scanning mirror settings are under the control of a microprocessor.

The transmission factors of the three optical interference filters are shown in Figure 1, and the blackbody radiance curves, taking into account the filter transmittance, are shown in Figure 2. Note that the 8.62- $\mu\text{m}$  filter transmits only about half of the energy of the other two filters.

All radiometer functions are controlled by a PC. These functions include the selector mirror position, the aperture setting, filter setting, shutter setting, analog gain, integrator setting, hot reference blackbody temperature, calibration cycle, and the detector and calibration dewar level sensors.

## Performance of the ARM Radiometer

The performance of a radiometer is defined in terms of the minimum detectable radiance (*mdr*) above the system noise. The *mdr* depends on the optical aperture of the radiometer and the response and noise levels of the

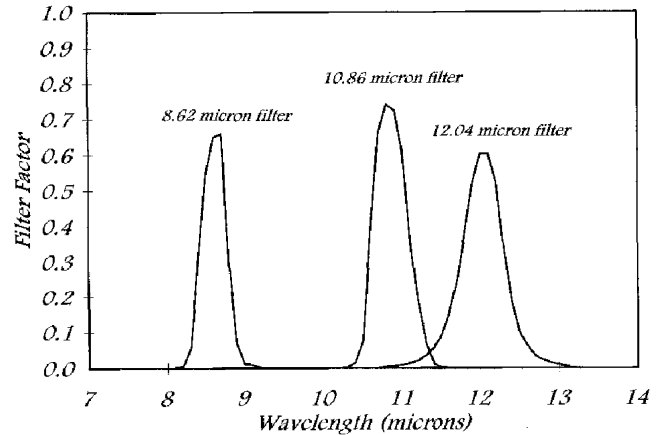


Figure 1. The radiometer filter transmittance factors.

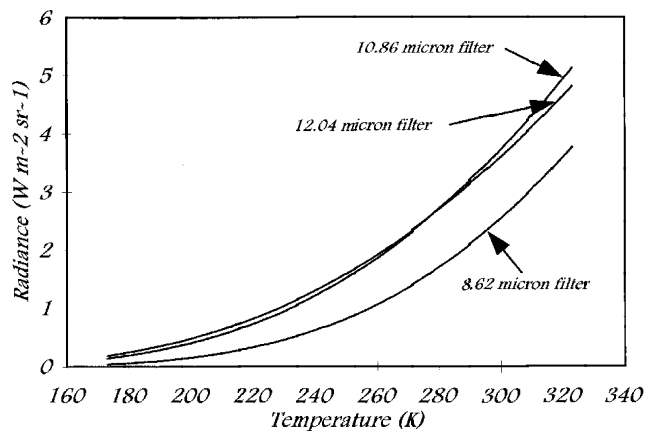


Figure 2. Blackbody radiances for the three filter channels.

detector and following electronics. The theoretical *mdr* was calculated from the radiometer primary aperture area, the field of view, and the noise equivalent power of the detector. The observational *mdr* was calculated by pointing the radiometer at a source of known radiance and measuring the signal and noise levels.

The observational tests were made under operational conditions during the PROBE experiment (see next section).

During PROBE the ARM radiometer was also compared over one day on January 29, 1993, against a CSIRO Mark II radiometer which had been operating successfully

for many years and which was also brought to PROBE to guard against periods when liquid nitrogen was not available. The CSIRO radiometer was an updated version of the original CSIRO Mark I radiometer (Platt 1971) that was used in the original LIRAD experiments (Platt 1973). The theoretical and observational *mdr*'s of the CSIRO Mark II were also calculated.

The radiance traces and noise levels for the two radiometers are shown in Figures 3 and 4. The most comparable part of the curves is from 1100 hr onwards, when the CSIRO and ARM radiometer filter spectral channels were most

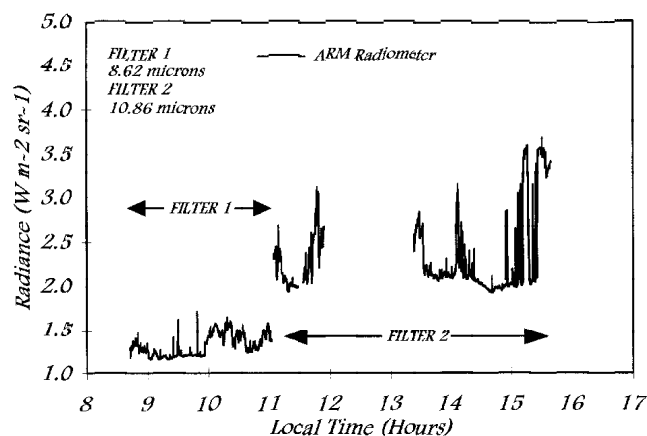


**Figure 3.** Infrared radiances measured by the ARM radiometer, January 29, 1993.

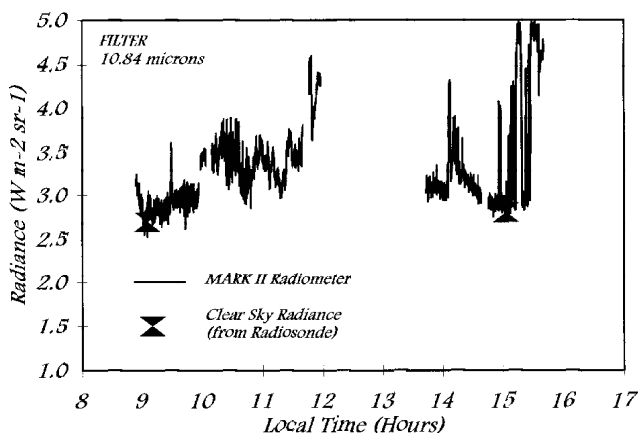


**Figure 4.** Infrared radiances measured by the CSIRO Mark II radiometer, January 29, 1993.

similar, although the filter transmittances and widths were different. The noise level of the ARM radiometer is obviously lower.

The theoretical and observational performances of the two radiometers are shown in Tables 1 and 2, respectively. The noise equivalent power (NEP) of the ARM detector is  $1.73 \times 10^{-2}$  lower than the value of the Mark II detector. The *mdr* of the ARM radiometer is similarly  $6.9 \times 10^{-3}$  lower. In the field, the ARM radiometer *mdr* is a factor of  $5.4 \times 10^{-2}$  lower than that of the CSIRO Mark II. However, both *mdr*'s are well above their theoretical values.

Since the Kavieng observations, the radiometer has been checked for spurious noise levels. Removal of an earth loop reduced the experimental *mdr* to  $3.58 \times 10^{-4} \text{ W m}^{-2} \text{ sr}^{-1} \text{ Hz}^{-1/2}$ , which is only a factor of 2 above the theoretical value. The remaining discrepancy was thought to be due to incomplete optical alignment of the final optical image on the detector. The performance of the Mark II under the tropical Kavieng field conditions was expected to be degraded because the ambient golay detector is susceptible to thermal gradients and drafts. It turned out also that the Mark II system had become slightly out of alignment on shipment to Kavieng.

However, the CSIRO Mark II performed sufficiently well to detect even thin cirrus above the system noise levels, and the ARM radiometer experimental *mdr* was lower than the Mark II theoretical value.

The radiometer will be described in more detail in a future technical paper.

## Observations of Tropical Cirrus

Observations were made at Kavieng, New Ireland, Papua New Guinea ( $2.5^\circ\text{S}$  latitude,  $152^\circ\text{E}$  longitude) as part of the ARM PROBE in January and February 1993. The CSIRO lidar and ARM radiometer made LIRAD observations (e.g., Platt et al. 1987) of cirrus and midlevel clouds in the vertical together with interferometric and microwave observations made by the NOAA ETL. Radiosonde data were also available every 6 hours.

Typical radiance data obtained are shown in Figures 3 and 4 for the ARM and CSIRO Mark II radiometers, respectively. The ARM radiometer detected at  $8.62 \mu\text{m}$  before 11 a.m.

**Table 1.** Theoretical performances of the CSIRO ARM and Mark II Radiometers.

Radiometer	Aperture Area (m <sup>2</sup> )	Field of View (sr)	Noise Equivalent Power (W Hz <sup>-1/2</sup> )	Minimum Detectable Radiance (W m <sup>-2</sup> sr <sup>-1</sup> Hz <sup>-1/2</sup> )
ARM	8.24x10 <sup>-4</sup>	4.07x10 <sup>-5</sup>	5.2x10 <sup>-12</sup>	1.55x10 <sup>-4</sup>
Mark II	4.71x10 <sup>-4</sup>	2.83x10 <sup>-5</sup>	3x10 <sup>-10</sup>	2.25x10 <sup>-2</sup>

**Table 2.** Experimental performances of the CSIRO ARM and Mark II radiometers at PROBE, Kavieng.

Radiometer	Signal <sup>(a)</sup> (Arbitrary)	RMS Noise (Arbitrary)	Signal to Noise Ratio <sup>(b)</sup>	Source Radiance <sup>(a)</sup> (W m <sup>-2</sup> sr <sup>-1</sup> )	Minimum Detectable Radiance (W m <sup>-2</sup> sr <sup>-1</sup> Hz <sup>-1/2</sup> )
ARM <sup>(c)</sup>	26,866	10.85	2,442(1)	4.477	3.67x10 <sup>-3</sup>
Mark II	2,040	10.2	200.0(5)	6.040	1.34x10 <sup>-1</sup>
ARM <sup>(d)</sup>	30,000	1.2	25,000(1)	4.477	3.58x10 <sup>-4</sup>

(a) Calibration: liquid nitrogen against 40°C Chopper reference blackbody

(b) Electronic time constant ( $\tau$ ) in parentheses. Note that the bandwidth in Hz is given by  $\sqrt{4\tau}$ .

(c) ARM radiometer operating at Kavieng.

(d) ARM radiometer after earth loop removal at Aspendale.

and at 10.86  $\mu\text{m}$  after that time. The CSIRO radiometer detected at 10.84  $\mu\text{m}$  for the whole period. The variable signals reflect the variable cloud types which were overhead during the day. The clear sky radiance levels are also shown in Figure 2. The radiances greater than 4 W m<sup>-2</sup> sr<sup>-1</sup> represent cumulus cloud episodes, while in between are variable cirrus and altocumulus.

A comparison of the ARM radiances and those obtained by the NOAA ETL interferometer is shown in Figure 5. The ETL radiances were obtained by integrating the output spectra over the radiometer filter functions. Considering the variable radiances over the comparison period, the correspondence is very good and points to confidence in the calibration of the two instruments.

The use of the ETL microwave data is shown in Figures 6 and 7. The changes in the water vapor column as measured with the ETL microwave radiometer can be converted into

radiances by calculating the radiances at the times of the radiosondes and fitting them to the column water vapor. The resultant curve is shown in Figure 6, and the original water vapor column data in Figure 7.

Radiances measured on January 24 using the CSIRO Mark II radiometer (liquid nitrogen was not available on that day) are shown in Figure 8. The calculated clear sky radiances (from the radiosonde) are also shown. The change in radiance occurring after 1700 hrs LT is seen to be due largely to changes in water vapor column rather than cloud, although there were thin cirrus on that day. The large changes in water vapor radiance, comparable to those from cirrus clouds, are evident; and they emphasize the need for the microwave observations of water vapor in the very moist tropical climate encountered.

Figure 9 shows the radiance from deep cirrus cells which developed during the day of February 4, but dissipated

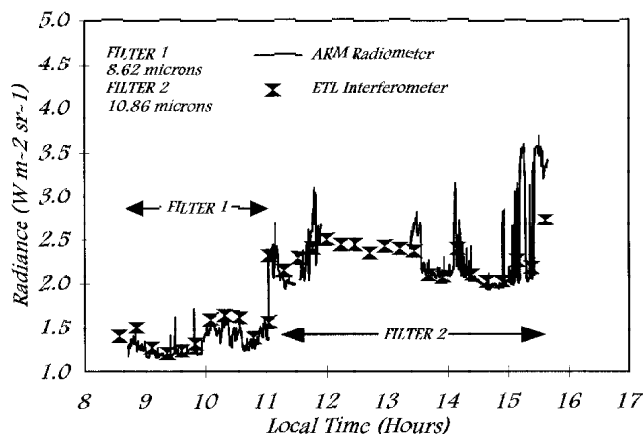


**Figure 5.** Comparison of radiances measured by the ARM radiometer and NOAA ETL radiometer, January 29th, 1993.

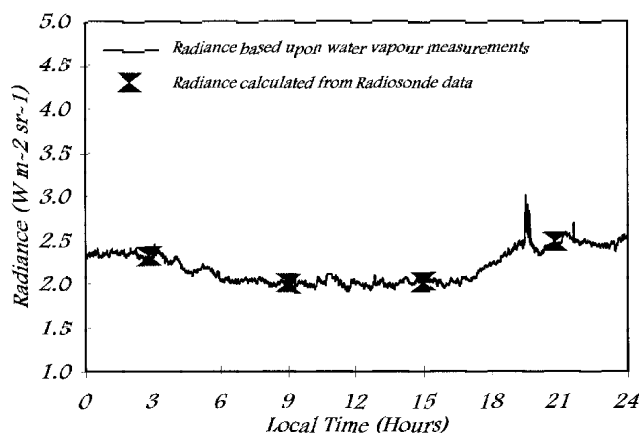


**Figure 6.** Changes in water vapor radiance calculated from the radiosonde and NOAA ETL microwave radiometer, January 24, 1993.

towards the evening. Using the LIRAD method, the integrated attenuated backscatter (e.g., Platt et al. 1987) was calculated for a number of lidar shots covering the period from about 1350 to 1430 hrs LT and is shown plotted together with infrared emittance in Figure 10. The integrated backscatter and emittance are quite well correlated. The cirrus has an emittance which varies from close to unity at the center of a cell to close to zero at the edge. In this particular analysis, changes in clear sky radiance that are

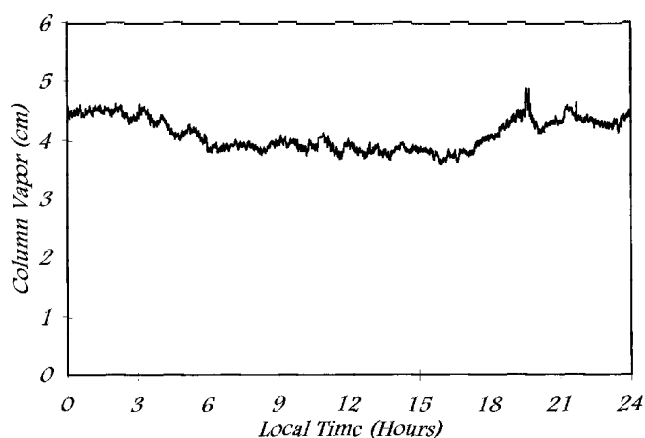


**Figure 7.** Changes in water vapor column from which the radiances in Figure 5 were calculated, January 24, 1993.

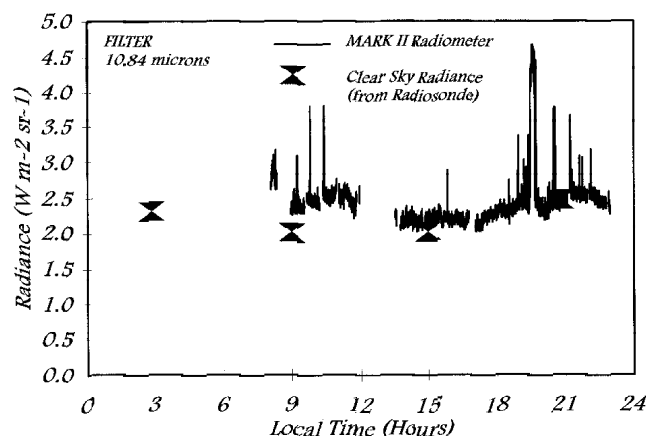


**Figure 8.** Infrared radiances measured with the CSIRO Mark II radiometer, January 24, 1993.

due to water vapor changes have not been taken into account, although the water vapor radiance and transmittance were fully accounted for. The integrated attenuated backscatter of  $0.02 \text{ sr}^{-1}$  when the emittance tends to unity compares with tropical values of  $0.025 \text{ sr}^{-1}$  Platt et al. (1987) obtained at Darwin, N. Australia.

Values of integrated backscatter were calculated from calibrated cirrus lidar returns at  $0.532 \mu\text{m}$ .

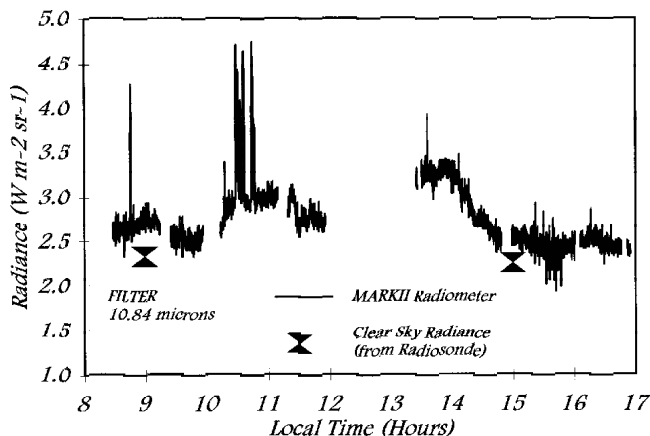


**Figure 9.** Infrared radiances measured by the CSIRO Mark II radiometer, February 4, 1993.

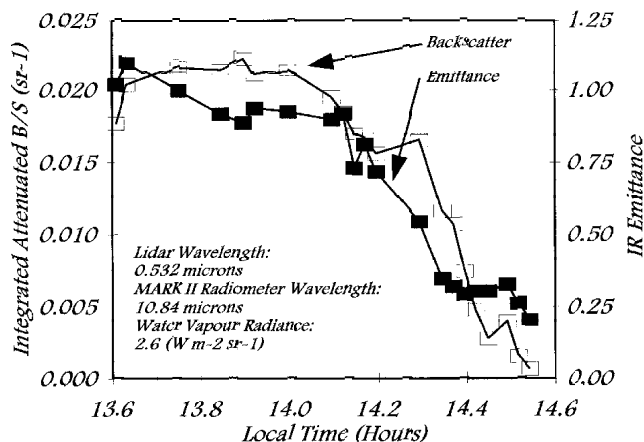


**Figure 10.** Lidar integrated backscatter and infrared emittance plotted against local time, February 4th, 1993.

## Future Developments

The ARM radiometer is now being duplicated but with the present detector liquid nitrogen dewar replaced by a Stirling cycle cooling system. This modification will make the radiometer independent of liquid nitrogen supplies. In

that case, calibration is effected against a blackbody at ambient temperature. It is intended that the new version be suitable for installation at ARM Cloud and Radiation Testbed sites.

The LIRAD method will also be extended to encompass methods of obtaining ice crystal habit, both from the integrated backscatter and from the measurement of the linear depolarization ratio. Information on cloud particle size will be obtained from the *shape* of the curve of integrated backscatter versus emittance.

## Acknowledgments

Stephen Marsden analyzed the lidar and radiometer data. John Bennett oversaw the design and construction of the radiometer. Reg Henry assisted considerably with the construction of the radiometer and with its siting and initial operation at Kavieng.

## References

- Platt, C.M.R. 1971. A narrow-beam radiometer for atmospheric radiation studies. *J. Appl. Met.* **10**:1307-1313.
- Platt, C.M.R. 1973. Lidar and radiometric observations of cirrus clouds. *J. Atmos. Sci.* **30**:1191-1204.
- Platt, C.M.R., J. C. Scott, and A. C. Dilley. 1987. Remote sounding of high clouds. Part VI: Optical properties of midlatitude and tropical cirrus. *J. Atmos. Sci.* **44**:729-747.
- Platt, C.M.R., and Harshvardhan. 1988. Temperature dependence of cirrus extinction: Implications for climate feedback. *J. Geophys. Res.* **93**:11051-11058.
- Platt, C.M.R., J. W. Bennett, S. A. Young, M. D. Fenwick, P. J. Manson, G. R. Patterson, and B. Petraitis. 1994. Narrow-beam fast filter radiometry and the use of the lidar/radiometer method in the Atmospheric Radiation Measurement Program. *Proceedings of the Third Atmospheric Radiation Measurement (ARM) Science Team Meeting, March 1-4, 1993, Norman, Oklahoma*, pp. 293-297. CONF-9303112, U.S. Department of Energy, Washington, D.C.